Equatorial Planetary Waves and Their Signature in Atmospheric Variability

KEVIN M. GRISE AND DAVID W. J. THOMPSON

Department of Atmospheric Science, Colorado State University, Fort Collins, Colorado

ABSTRACT

Equatorial planetary waves are a fundamental component of the tropical climate system. Previous studies have examined their structure in the climatological-mean circulation, their role in the climatological-mean momentum balance of the tropics, and their contribution to the climatological-mean upwelling across the tropical tropopause. In this study, the authors focus on the contribution of the equatorial planetary waves to variability in the tropical circulation about its climatological-mean state.

The equatorial planetary waves that dominate the climatological mean exhibit considerable variability on intraseasonal and interannual time scales. Variability in the amplitude of the equatorial planetary waves is associated with a distinct pattern of equatorially symmetric climate variability that also emerges from empirical orthogonal function analysis of various tropical dynamical fields. Variability in the equatorial planetary waves is characterized by variations in 1) convection in the deep tropics, 2) eddy momentum flux convergence and zonal-mean zonal wind in the tropical upper troposphere, 3) the mean meridional circulation of the tropical and subtropical troposphere, 4) temperatures in the tropical lower stratosphere and subtropical troposphere of both hemispheres, and 5) the amplitude of the upper tropospheric anticyclones over the western tropical Pacific Ocean.

It is argued that pulsation of the equatorial planetary waves provides an alternative framework for interpreting the response of the tropical circulation to a range of climate phenomena. Pulsation of the equatorial planetary waves is apparent in association with opposing phases of El Niño–Southern Oscillation and select phases of the Madden–Julian oscillation. Pulsation of the equatorial planetary waves also contributes to variability in measures of the width of the tropical belt.

1. Introduction

Zonal asymmetries, or eddies, play a fundamental role in the atmospheric general circulation. In the extratropics, baroclinic eddies are generated near the surface in regions of large horizontal temperature gradients and propagate vertically in the troposphere and meridionally in the vicinity of the tropopause (e.g., Simmons and Hoskins 1978; Edmon et al. 1980). The heat and momentum fluxes associated with the eddies are crucial in maintaining key aspects of midlatitude climate, including the surface westerlies and the horizontal distribution of temperature.

In the tropics, baroclinic instability is inhibited by weak rotation and small horizontal temperature gradients. Here, quasi-stationary equatorial planetary waves forced by the latent heat release from deep convection play a key role in the large-scale atmospheric circulation. Equatorial planetary waves are readily observed in the climatological-mean tropical circulation and are dominated by 1) an equatorially trapped Rossby wave response to the west of convective heating over the western tropical Pacific Ocean and 2) a Kelvin wave response to the east of the heating (e.g., Dima et al. 2005; Dima and Wallace 2007). The observed equatorial planetary waves strongly resemble the idealized model response to a localized midtropospheric heat source centered on the equator (e.g., Gill 1980; Highwood and Hoskins 1998). The equatorial planetary waves propagate vertically, achieving their maximum amplitude in the tropical upper troposphere (e.g., Dima and Wallace 2007) before becoming evanescent at stratospheric levels (Dunkerton 1995).

As is the case for baroclinic eddies in the extratropics, equatorial planetary waves play an important role in the momentum balance of the atmosphere. In the upper troposphere, the equatorial Rossby wave pattern is tilted

Corresponding author address: Kevin M. Grise, Dept. of Atmospheric and Oceanic Sciences, McGill University, 805 Sherbrooke St. West, Montreal, QC H3A 2K6, Canada.
E-mail: kevin.grise@mcgill.ca

meridionally, such that the Rossby waves propagate out of the deep tropics and flux westerly momentum into the equatorial upper troposphere (e.g., Dima et al. 2005). As a result, model experiments that include zonally asymmetric heating in the tropics—and thus generate equatorial planetary waves—often produce upper tropospheric westerly winds (superrotation) centered about the equator (Kraucunas and Hartmann 2005). The observed easterlies in the tropical upper troposphere are driven not by the equatorial planetary waves (which provide a westerly torque in the tropical upper troposphere) but rather by the easterly torque associated with the seasonal cycle in the upper tropospheric cross-equatorial flow (Lee 1999; Dima et al. 2005; Kraucunas and Hartmann 2005).

Equatorial planetary waves may also be important in driving a component of the long-term mean upwelling at the tropical tropopause. Until recently, the long-term mean and seasonal cycle of temperatures in the tropical lower stratosphere have been explained almost exclusively in the context of upwelling driven by the zonal-mean balanced response to planetary wave breaking in the extratropical stratosphere (Yulaeva et al. 1994; Holton et al. 1995; Ueyama and Wallace 2010). However, several recent studies have proposed that the upwelling is also influenced by the eddy momentum flux convergence associated with equatorial planetary waves (Boehm and Lee 2003; Kerr-Munslow and Norton 2006; Norton 2006; Randel et al. 2008; Ryu and Lee 2010). In this case, the seasonal cycle in tropical upwelling is due not to the seasonal cycle in Northern Hemisphere stratospheric wave breaking but to either 1) the seasonal cycle in the latitude of tropical convection (Norton 2006) or 2) the seasonal cycle in the height of tropical convection and its associated wave response (Randel et al. 2008). To date, the exact role of equatorial planetary waves in tropical upwelling remains unresolved.

Hence, it is becoming increasingly clear that equatorial planetary waves play a fundamental role in the tropical climate system. Most previous studies of equatorial planetary waves have focused on their role in the long-term mean and seasonal cycle of the tropical circulation. In this study, we focus instead on the role of equatorial planetary waves in driving variability about the seasonal cycle. We demonstrate that variations in the equatorial planetary waves are associated with a distinct pattern of equatorially symmetric climate variability that plays a key role in the interannual and intraseasonal variability of the tropical circulation. In section 2, we describe the data and methods used in this study. In section 3, we review the climatological-mean structure of the equatorial planetary waves and identify a simple index of the amplitude of the waves based on

the eddy zonal wind field in the tropics. We analyze the signature of the equatorial planetary waves in various atmospheric fields in section 4. We then consider the linkages between the equatorial planetary waves and a range of tropical phenomena. Section 5 examines the linkages between the equatorial planetary waves, the El Niño–Southern Oscillation (ENSO), and the Madden–Julian oscillation (MJO); section 6 examines the linkages between the equatorial planetary waves and variability in the width of the tropics and stratosphere–troposphere exchange. Section 7 concludes with a summary of the key results.

2. Data and methods

a. Data

The primary data used in this study are temperatures, geopotential heights, and winds from the National Centers for Environmental Prediction (NCEP)–National Center for Atmospheric Research (NCAR) reanalysis dataset (Kalnay et al. 1996), outgoing longwave radiation (OLR) from the National Oceanic and Atmospheric Administration (NOAA) interpolated OLR dataset (Liebmann and Smith 1996), and sea surface temperatures (SSTs) from version 2 of the NOAA Optimal Interpolation SST dataset (OISST; Reynolds et al. 2002). All three datasets are obtained from the Physical Sciences Division of the NOAA Earth System Research Laboratory. The reanalysis data are restricted to the period following 1979 when more comprehensive satellite data are included in the reanalysis data assimilation scheme (Kalnay et al. 1996; Kistler et al. 2001). The results of this study focus on the period through the end of 2009.

Water vapor concentrations in the stratosphere and upper troposphere are taken from the Earth Observing System *Aura* Microwave Limb Sounder (MLS) version 2.2 water vapor data (Lambert et al. 2007; Read et al. 2007). The data are obtained from the National Aeronautics and Space Administration (NASA) Jet Propulsion Laboratory and begin in August 2004. The MLS instrument measures water vapor concentrations using naturally occurring thermal emissions from the microwave spectrum and provides approximately 3500 profiles per day covering the region equatorward of 82° latitude in each hemisphere. The corresponding satellite tracks have approximately 200 km × 7 km horizontal resolution and are separated by 10°–20° longitude at mid- and low latitudes. The data have approximately 3.5-km vertical resolution near the tropopause.

b. Methods

In this paper, we make extensive use of the expansion coefficient time series of various spatial patterns. The

temporal variability of spatial pattern $P(x)$ in dataset $A(t, x)$ is found via projection as

$$y(t) = A(t,x)P(x) \qquad (1)$$

where x denotes the spatial dimension and t denotes the time dimension. By construction, the time series $y(t)$ reflects the temporally varying amplitude of $P(x)$ in $A(t, x)$. Prior to the projection, all data in P and A are weighted by the square root of the cosine of the latitude (if the data contain a meridional spatial dimension) and the square root of the long-term mean density (if the data contain a vertical spatial dimension). [Multiplying the data by the square root of the cosine of the latitude is equivalent to multiplying the projection in (1) by the cosine of the latitude.] In the case of empirical orthogonal function (EOF) analysis, $P(x)$ represents an EOF found from eigenanalysis of the covariance matrix of A, and $y(t)$ is the associated principal component (PC) time series.

The statistical significance of the regression coefficient between two time series is estimated by testing whether the associated correlation coefficient is significantly different from zero. The test is performed using Student's t statistic applied to the correlation coefficient r with $n^* - 2$ degrees of freedom:

$$t = r\sqrt{\frac{n^* - 2}{1 - r^2}}. \qquad (2)$$

The effective sample size n^* is estimated using the relation

$$n^* = n\frac{1 - r_1 r_2}{1 + r_1 r_2}, \qquad (3)$$

where n is the number of samples and r_i is the lag-1 autocorrelation for the time series i (Bretherton et al. 1999).

Eddy kinetic energy is defined as

$$\frac{1}{2}(u^{*2} + v^{*2}), \qquad (4)$$

where u is the zonal wind, v is the meridional wind, and the asterisks represent deviations from the zonal mean.

The eddy momentum flux is similarly defined as u^*v^*. Both the eddy kinetic energy and eddy momentum flux are calculated using 6-hourly NCEP–NCAR reanalysis data and then averaged to form daily and monthly means as required.

The mean meridional mass streamfunction is defined as

$$\frac{2\pi a \cos\phi}{g}\int_0^p [v]\, dp, \qquad (5)$$

where a is Earth's radius, ϕ is the latitude, g is the acceleration of gravity, and the square brackets indicate the zonal mean. The values of the streamfunction are constrained to vanish at the lower boundary.

Unless otherwise noted, the term *anomalous* refers to a time series in which the seasonal cycle and the long-term trend have been removed from the data so that the variance associated with the annual cycle (i.e., the long-term mean as a function of calendar day) and the long-term trend does not contribute to the results. The term *standardized* refers to a time series with a mean of zero and a standard deviation of one.

To characterize ENSO variability, we use the standardized leading PC time series of monthly-mean sea surface temperature anomalies over the tropical Pacific Ocean (30°N–30°S, 120°E–60°W) (e.g., Hoerling et al. 2001). The resulting PC time series is referred to herein as the ENSO index time series. By definition, positive values of the PC time series correspond to the warm phase of the ENSO cycle, and vice versa.

To characterize variability in the MJO, we use the paired MJO indices obtained from the Bureau of Meteorology Research Centre of The Centre for Australian Weather and Climate Research (i.e., the so-called "real-time multivariate MJO indices," or RMM1 and RMM2). The MJO index time series represent the first two PCs of the combined 15°N–15°S-averaged 850-hPa zonal wind, 200-hPa zonal wind, and OLR fields with the interannual variability removed (Wheeler and Hendon 2004).

3. Defining temporal variability in the equatorial planetary waves

In this section, we first review the structure of the equatorial planetary waves in the climatological-mean circulation. We then develop an index that describes temporal variability in the amplitude of the climatological-mean pattern of equatorial planetary waves. The index is found by projecting upper tropical tropospheric circulation anomalies onto the climatological-mean structure of the equatorial planetary waves.

a. Structure of the equatorial planetary waves in the climatological-mean circulation

The top panel in Fig. 1 shows the climatological-mean geopotential height and wind fields at 150 hPa. At this level, the structure of the climatological-mean circulation in the tropics is clearly dominated by equatorial planetary waves (e.g., Dima and Wallace 2007). Over the western Pacific Ocean, the mean circulation in the
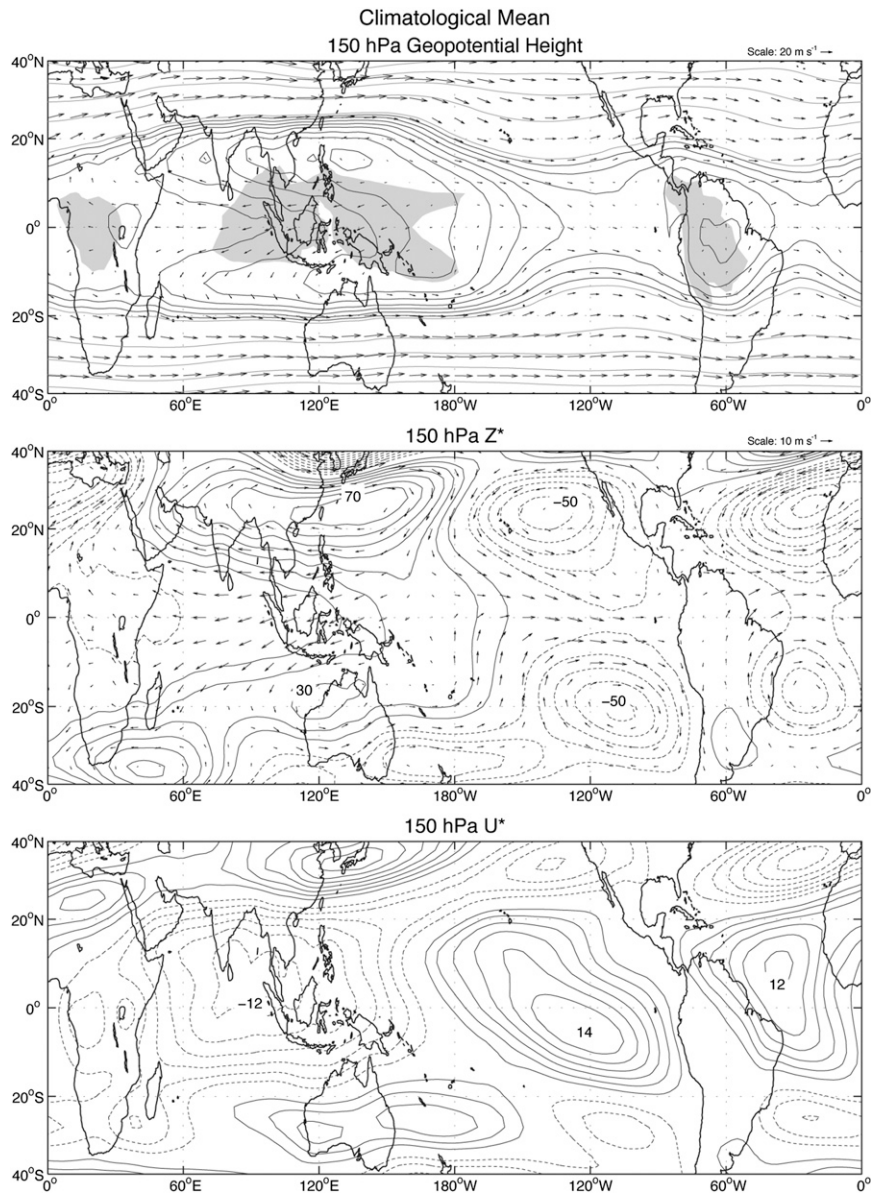
FIG. 1. Climatological-mean (top) 150-hPa geopotential height contours and wind vectors, (middle) 150-hPa Z^* contours and eddy wind vectors, and (bottom) 150-hPa U^* contours. (Z^* and U^* denote the eddy components of the geopotential height and zonal wind fields, respectively; i.e., the zonal mean has been removed from each of these fields.) The contour interval is (top) 100 m for the gray contours (values $\leq$ 14 200 m) and 10 m for the black contours (values $\geq$ 14 210 m), (middle) 10 m, and (bottom) 2 m s^{-1}. Positive contours are solid, negative contours are dashed, and the zero contour is omitted. The shaded regions in the top panel denote regions with outgoing longwave radiation values less than 230 W m^{-2}. Unless otherwise noted, all figures in this paper are based on data covering the period 1979–2009.

tropics strongly resembles the idealized model response to a localized tropical heat source, with off-equatorial anticyclonic gyres to the west of the convection over the western tropical Pacific Ocean and a Kelvin wave response to the east of the convection (e.g., Gill 1980; Highwood and Hoskins 1998; Norton 2006). The mean

circulation in the tropics also includes the wave responses to the climatological-mean heat sources over Africa and South America.

The middle panel in Fig. 1 shows the eddy component of the climatological-mean geopotential height and wind fields at 150 hPa (removing the zonal mean
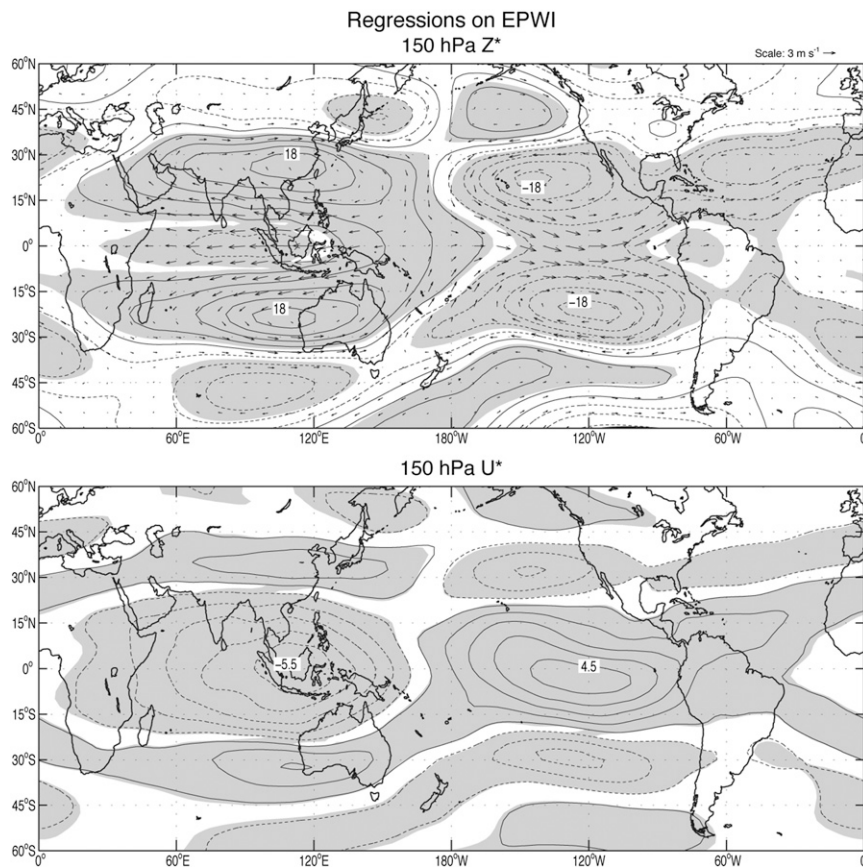
FIG. 2. Regressions of daily-mean anomalies on the EPWI time series: (top) 150-hPa Z^* (contours) and eddy winds (vectors) and (bottom) 150-hPa U^*. Positive contours are solid; negative contours are dashed. The contour interval is (top) 4 m $(-6, -2, 2, 6, ...)$ and (bottom) 1 m s^{-1} $(-1.5, -0.5, 0.5, 1.5, ...)$. Units are per standard deviation in the EPWI time series. The shading indicates regions that are 95% significant.

accentuates the zonally asymmetric structures inherent in the climatological-mean circulation). The 150-hPa Z^* field is dominated by paired off-equatorial anticyclones over the western Pacific Ocean and paired off-equatorial cyclones over the eastern Pacific and Atlantic Oceans. The associated eddy wind field is dominated by easterlies over the tropical Indian and western Pacific Oceans and westerlies over the tropical eastern Pacific and Atlantic Oceans (see also the bottom panel in Fig. 1).

b. Quantifying temporal variability in the equatorial planetary waves

Temporal variability in the amplitude of the climatological-mean pattern of equatorial planetary waves is quantified by projecting the anomalous eddy zonal wind field at 150 hPa (i.e., the anomalous 150-hPa U^* field) onto the seasonally varying climatological-mean 150-hPa U^* field over the domain 20°N–20°S. The underlying assumption here is that the climatological-mean 150-hPa

U^* field is dominated by the structure of the equatorial planetary waves in the deep tropics (see Dima and Wallace 2007). Additionally, we use the seasonally varying climatological-mean of the 150-hPa U^* field (rather than the annual mean shown in the bottom panel of Fig. 1) to account for seasonal changes in the structure of the equatorial planetary waves. The resulting projection time series is hereafter referred to as the equatorial planetary wave index (EPWI). As discussed below, very similar indices can be derived from EOF analysis of a range of tropical dynamical fields. Note that both stationary and transient U^* anomalies contribute to the variability described by the EPWI time series.

Figure 2 shows the maps formed by regressing daily-mean 150-hPa Z^* and eddy wind anomalies onto standardized values of the EPWI time series. By construction, the results are reminiscent of the long-term mean structure of the equatorial planetary waves (Fig. 1; Dima et al. 2005; Dima and Wallace 2007). Positive values of the EPWI time

series (i.e., enhanced amplitude in the equatorial planetary waves) are associated with paired 150-hPa anticyclones and cyclones that straddle the equator over the Pacific Ocean, easterlies over the tropical Indian and western Pacific Oceans, and westerlies over the tropical eastern Pacific Ocean.

The EPWI time series describes the pulsation of the climatological-mean pattern of equatorial planetary waves, particularly over the Indian and Pacific Ocean basins. That the EPWI time series and thus the structures in Fig. 2 reflect a coherent pattern of large-scale variability in the tropical atmosphere is supported by two facts. First, similar structures emerge from one-point correlation maps based on the upper tropical tropospheric circulation. For example, the top panel of Fig. 3 shows one-point correlations of daily 150-hPa U^* anomalies using a base point over the Maritime Continent. By construction, the 150-hPa U^* anomalies over the Maritime Continent are significantly correlated with themselves, but they are also significantly correlated with 150-hPa U^* anomalies throughout the tropics. (Similar results are found using a base point over the tropical eastern Pacific Ocean.) The spatial distribution of the significant point correlations (Fig. 3, top) clearly resembles that of the regression pattern shown in Fig. 2 (bottom). As discussed further in section 5, the structure of the equatorial planetary waves is clearly apparent on interannual and intraseasonal time scales but less so on submonthly time scales (Fig. 3, bottom three panels).

Second, the EPWI time series is closely related to the leading PC time series of various tropical dynamical fields (and is not sensitive to the exact latitude bounds chosen for the data projection). As documented in Table 1, the EPWI time series is strongly correlated with the PC time series of the tropical eddy kinetic energy field, zonal wind field, and the eddy components of the geopotential height and temperature fields.

The results in this section thus reveal that

1) Variability in the amplitude (i.e., pulsing) of the climatological-mean pattern of equatorial planetary waves can be quantified by projecting tropical 150-hPa U^* anomalies onto the seasonally varying climatological-mean 150-hPa U^* field.

2) The resulting projection time series (referred to as the EPWI time series) is associated with a distinct pattern of climate variability that also emerges from one-point correlation maps and from EOF analysis of a range of tropical dynamical fields.

In the next section, we explore and diagnose the structures associated with the EPWI time series in further detail.

4. Signatures of temporal variability in the equatorial planetary waves

In this section, we examine the structures associated with temporal variability in the amplitude of the climatological-mean pattern of equatorial planetary waves by regressing various zonal-mean and zonally varying fields onto standardized values of the EPWI time series. Zonal-mean results are shown in Fig. 4, and zonally varying results are shown in subsequent figures (Figs. 5 and 7). Note that the Z^* and eddy wind regressions shown in Fig. 5 (top) are reproduced from Fig. 2 (top) for the purpose of comparison.

Periods of enhanced amplitude in the equatorial planetary waves (i.e., the positive polarity of the EPWI time series) are associated with equatorward eddy momentum flux anomalies in the tropical upper troposphere of both hemispheres (Fig. 4, top left). The equatorward eddy momentum flux anomalies evident in the zonal mean arise largely from a meridional couplet over the Maritime Continent (Fig. 5, middle) and are consistent with the meridional tilt of the eddy wind vectors in that region (Fig. 5, top). The pattern of the tropical eddy momentum flux anomalies in Fig. 4 (top left) is similar to that associated with the modeled equatorial planetary wave response to localized midtropospheric diabatic heating centered on the equator (Kraucunas and Hartmann 2005; Norton 2006).

The results in Fig. 4 (top left) also suggest that the EPWI time series is associated with eddy momentum flux anomalies in the upper troposphere at extratropical latitudes. Hence, variations in the amplitude of the equatorial planetary waves are seemingly linked to variability in the extratropical fluxes of momentum. The causal nature of these linkages is unclear, but it is worth noting that a similar pattern of extratropical eddy momentum fluxes is found in the idealized modeling experiments of Kraucunas and Hartmann (2005; cf. the transient eddy momentum fluxes in their Fig. 7c).

The pattern of zonal-mean zonal wind anomalies associated with variability in the equatorial planetary waves (Fig. 4, top right) is consistent with forcing by the eddy momentum flux anomalies in Fig. 4 (top left). Westerly wind anomalies are found in the tropical upper troposphere in the region of anomalous eddy momentum flux convergence, and easterly wind anomalies are found throughout the depth of the subtropical troposphere in both hemispheres. The barotropic component of the subtropical easterly wind anomalies is mandated by the anomalous divergence of the eddy momentum fluxes near 20° latitude. The upper tropospheric zonal-mean zonal wind anomalies arise primarily from the eastern Pacific Ocean sector (Fig. 5, bottom) and are associated
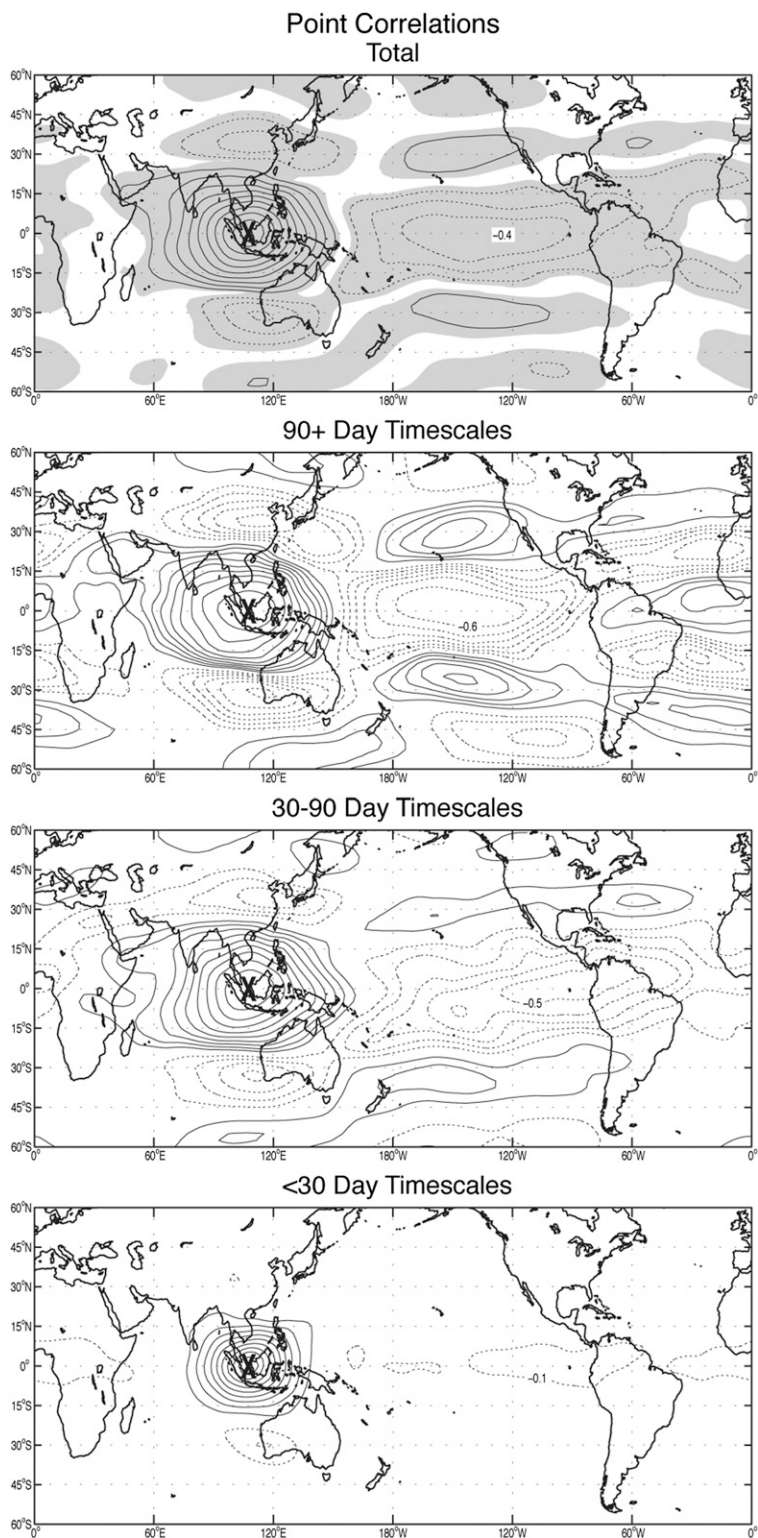
Point Correlations
Total

90+ Day Timescales

30-90 Day Timescales

<30 Day Timescales

FIG. 3. Point correlations of daily-mean 150-hPa U^* anomalies with the 150-hPa U^* anomaly at 0°N, 107.5°E (marked by "X"). The contour interval is 0.1. Positive contours are solid, negative contours are dashed, and the zero contour is omitted. (row 1) The shading indicates regions that are 95% significant. (rows 2–4) The correlations are derived from 150-hPa U^* anomalies that have been filtered according to time scale.

TABLE 1. Correlations with the EPWI time series. The correlations are calculated using daily values for the first eight indices and monthly values for the ENSO index time series. All PC time series listed in the table are derived using data from the region 20°N–20°S. The asterisk indicates that the zonal mean has been removed from a field. EKE refers to eddy kinetic energy [see Eq. (4)]. All correlations listed in the table are 95% significant.

Index	Correlation with EPWI
PC 1 of 150-hPa EKE	0.81
PC 2 of 200-hPa U	0.77
PC 1 of zonal mean EKE over 1000–10 hPa (17 levels)	0.74
PC 1 + PC 2 of 100-hPa T^*	0.70
PC 1 + PC 2 of 150-hPa Z^*	0.69
Sum of MJO indices	0.66
EPWI derived from 30–90-day filtered 150-hPa U^*	0.65
EPWI derived from 90+-day filtered 150-hPa U^*	0.62
Inverted ENSO index	0.60

with the flow surrounding the anomalous upper tropospheric cyclones in each hemisphere (Fig. 5, top).

The patterns of zonal-mean temperature and meridional mass streamfunction anomalies associated with variability in the equatorial planetary waves (Fig. 4, bottom row) are also consistent with forcing by the eddy momentum flux anomalies (the linkages are summarized in the schematic in Fig. 6). The anomalous divergence of the momentum fluxes near 20° latitude is balanced by the Coriolis torque acting on anomalous poleward motion; the anomalous convergence of the momentum fluxes in the deep tropics is balanced by the Coriolis torque acting on anomalous equatorward motion (note that the balance does not hold right at the equator, where the Coriolis parameter goes to zero). The positive temperature anomalies in the subtropical troposphere near 30° latitude are consistent with adiabatic warming in the subsiding branches of the resulting meridional circulation cells, and the weak or slightly negative temperature anomalies near 15° latitude are consistent with the rising branches of the circulation cells. The weak temperature anomalies near the tropical tropopause are also generally consistent with the meridional convergence of the mass circulation near the tropical tropopause level. Overall, the structures associated with variability in the equatorial planetary wave amplitudes resemble the patterns of eddy momentum flux, zonal wind, and temperature evident in the numerical simulations of Kraucunas and Hartmann (2005).

Finally, the patterns of OLR and sea surface temperature anomalies associated with variability in the equatorial planetary waves are shown in Fig. 7. The top panel of Fig. 7 shows the regressions of daily mean OLR anomalies onto the standardized EPWI time series. Periods of anomalously large equatorial planetary wave amplitude are associated with enhanced convection (negative OLR anomalies) over the Maritime Continent and western tropical Pacific Ocean and suppressed convection (positive OLR anomalies) over the Indian Ocean and the eastern tropical Pacific Ocean. The geopotential height anomalies in Fig. 5 (top) are consistent with the wave response to the OLR field: that is, anomalously low OLR (anomalous heating) is associated with off-equatorial anticyclonic anomalies and anomalously high OLR (anomalous cooling) is associated with off-equatorial cyclonic anomalies. As revealed in the next section, the dipole in OLR anomalies between the western and eastern tropical Pacific Ocean is reminiscent of that associated with ENSO, and the dipole in OLR anomalies between the tropical Indian Ocean and the Maritime Continent is reminiscent of the MJO.

The bottom panel of Fig. 7 shows the corresponding regressions for monthly mean sea surface temperature anomalies. Periods of enhanced equatorial planetary wave amplitude are associated with warm sea surface temperature anomalies over the midlatitude Pacific Ocean in each hemisphere and cold sea surface temperature anomalies over the eastern equatorial Pacific Ocean. As discussed further in section 5, the tropical sea surface temperature anomalies are indicative of the expected linkage between the amplitude of the equatorial planetary waves and the phase of ENSO (e.g., Rasmusson and Carpenter 1982).

The results in this section reveal that variations in the amplitude of the climatological-mean pattern of equatorial planetary waves are associated not only with upper tropospheric geopotential height and wind anomalies (Fig. 5, top and bottom panels), but also with a series of distinct equatorially symmetric features in the zonal-mean circulation. Prominent features observed in association with enhanced amplitude in the equatorial planetary waves include the following:

1) Anomalous eddy momentum flux convergence in the tropical upper troposphere and anomalous eddy momentum flux divergence in the subtropical upper troposphere (Fig. 4, top left)
2) Westerly zonal-mean zonal wind anomalies in the tropical upper troposphere and easterly zonal-mean zonal wind anomalies throughout the depth of the subtropical troposphere (Fig. 4, top right)
3) Positive zonal-mean temperature anomalies in the subtropical troposphere juxtaposed against negative zonal-mean temperature anomalies near the tropopause in both the tropics and the subtropics (Fig. 4, bottom left)
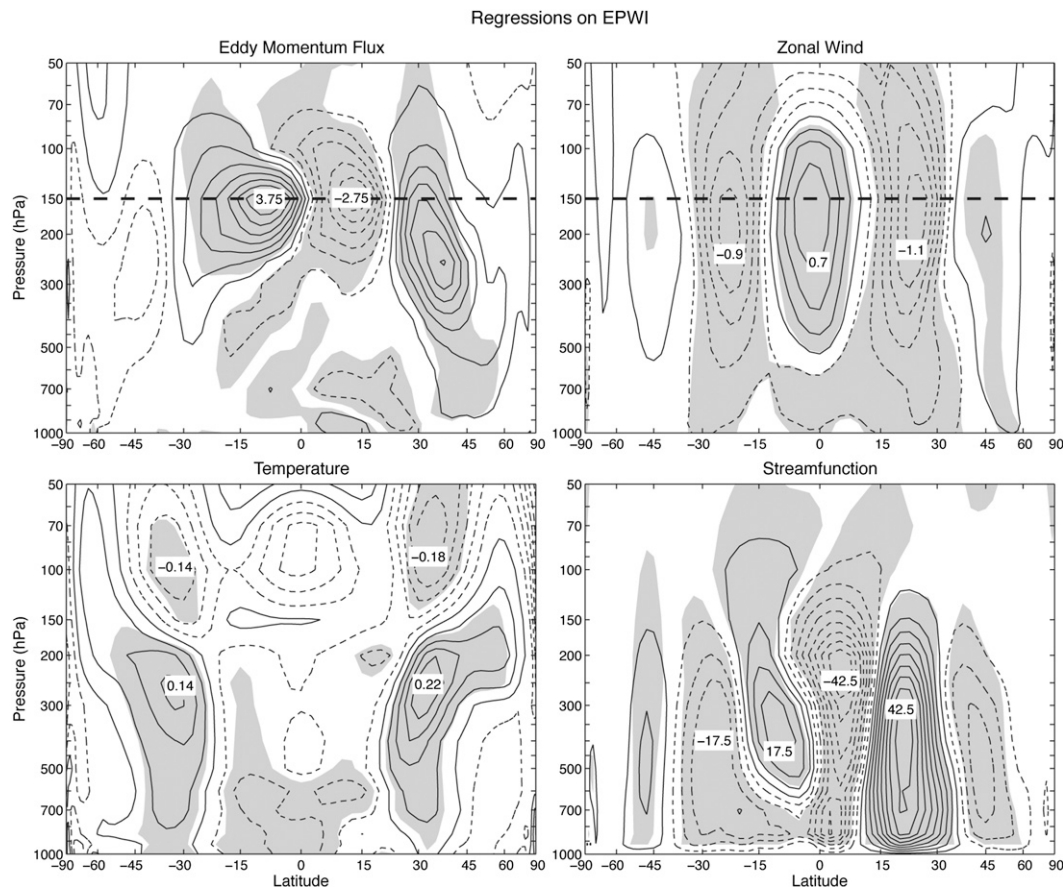
Regressions on EPWI

FIG. 4. Regressions of daily-mean, zonal-mean anomalies on the EPWI time series: (top left) eddy momentum flux, (top right) zonal wind, (bottom left) temperature, and (bottom right) mean meridional mass streamfunction (positive values indicate clockwise circulation). Positive contours are solid, and negative contours are dashed. The contour interval is (top left) 0.5 m^2 s^{-2} ($-0.75, -0.25, 0.25, 0.75, \ldots$), (top right) 0.2 m s^{-1} ($-0.3, -0.1, 0.1, 0.3, \ldots$), (bottom left) 0.04 K ($-0.06, -0.02, 0.02, 0.06, \ldots$), and (bottom right) 5×10^8 kg s^{-1} ($-7.5, -2.5, 2.5, 7.5, \ldots$). Units are per standard deviation in the EPWI time series. The shading indicates regions that are 95% significant. The thick dashed horizontal line in the top two panels denotes the level shown in the corresponding panels in Fig. 5. The contour labels in the bottom-right panel are in units of 10^8 kg s^{-1}. The abscissa in all panels of this figure and all subsequent figure panels with zonal-mean cross sections is plotted with a sine of latitude scale to accentuate the tropical features.

4) Anomalous meridional circulation cells in the troposphere of each hemisphere with rising motion near 15° latitude and sinking motion near the equator and 30° latitude (Fig. 4, bottom right)

5) OLR and sea surface temperature anomalies consistent with forcing of the equatorial planetary wave amplitudes by variations in atmospheric heating (Fig. 7).

5. Linkages between the equatorial planetary waves, ENSO, and the MJO

In this section, the relationship between variability in the amplitude of the equatorial planetary waves, ENSO, and the MJO is examined in the context of 1) the time scales that contribute to the structures associated with

the EPWI time series and 2) the comparison of the structures associated with the EPWI time series with those associated with ENSO and the MJO.

The time scales contributing to the structures associated with the EPWI time series are explored in Figs. 8 and 9. The top rows in Figs. 8 and 9 are identical: both show the regressions of zonal-mean eddy momentum flux and zonal wind (top left) and zonally varying 150-hPa Z^*, 150-hPa eddy winds, and OLR (top right) onto the standardized EPWI time series (the results are reproduced from previous figures to aid in the comparison between panels). The middle rows of Figs. 8 and 9 show the same fields as the top rows, but in this case, the basis for the regressions is the standardized projection time series derived by projecting time-filtered 150-hPa U^* anomalies onto the seasonally varying climatological-mean
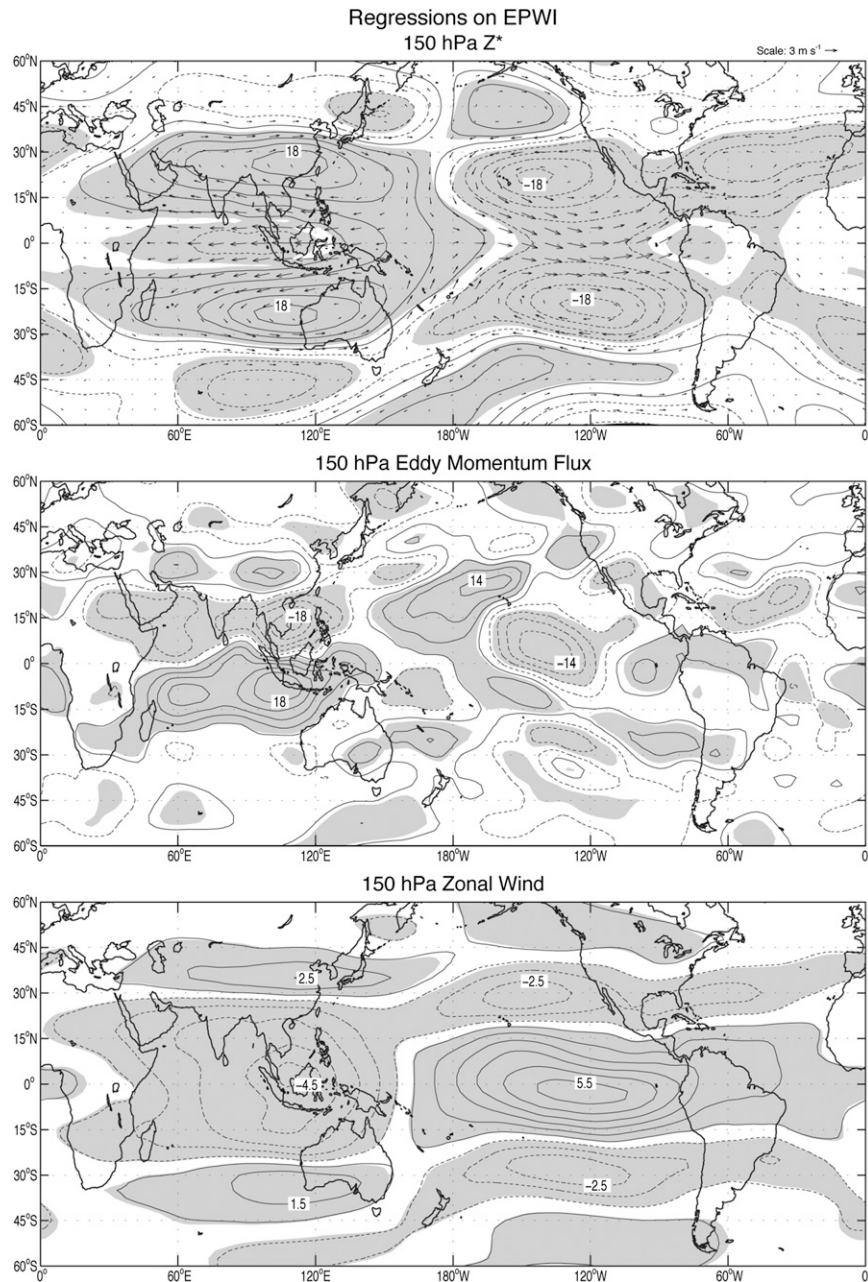
FIG. 5. As in Fig. 2, but for regressions of (middle) 150-hPa eddy momentum flux and (bottom) 150-hPa zonal wind. The contour interval is (middle) 4 $m^2 s^{-2}$ ($-6, -2, 2, 6, \ldots$), and (bottom) 1 $m s^{-1}$ ($-1.5, -0.5, 0.5, 1.5, \ldots$).

150-hPa U^* field over the domain 20°N–20°S (recall that the EPWI time series is derived by projecting unfiltered 150-hPa U^* anomalies onto the seasonally varying climatological-mean 150-hPa U^* field). The results in the middle row of Fig. 8 are based on 90-day low-pass filtered data; the results in the middle row of Fig. 9 are based on 30–90-day bandpass filtered data. The patterns associated with the projection time series derived from the 90-day

low-pass filtered 150-hPa U^* field (Fig. 8, middle row) and the 30–90-day bandpass filtered 150-hPa U^* field (Fig. 9, middle row) bear strong resemblance to the patterns associated with the EPWI time series (Figs. 8 and 9, top row). Thus, the structures associated with the EPWI time series arise from both intraseasonal and interannual time scales (see also one-point correlation maps in the bottom three panels of Fig. 3).
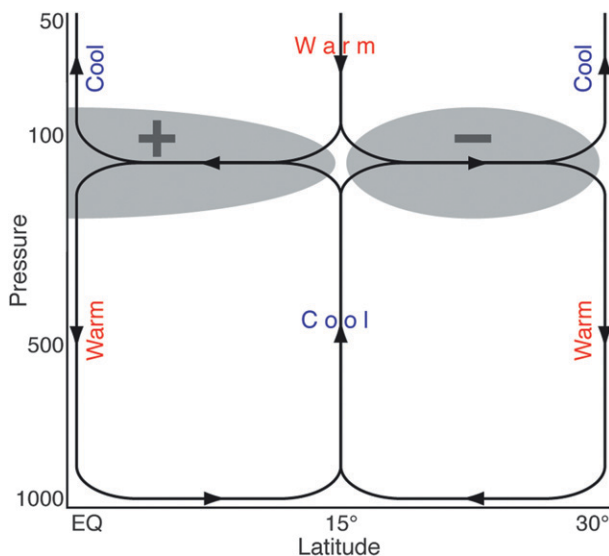
FIG. 6. Schematic of the transient equatorially symmetric zonal-mean processes associated with variability in the equatorial planetary waves. The gray circles signify regions of eddy momentum flux convergence (marked with a plus sign) and eddy momentum flux divergence (marked with a minus sign). The red and blue colors signify adiabatic warming and cooling, respectively. The vertical axis shows pressure levels (hPa).
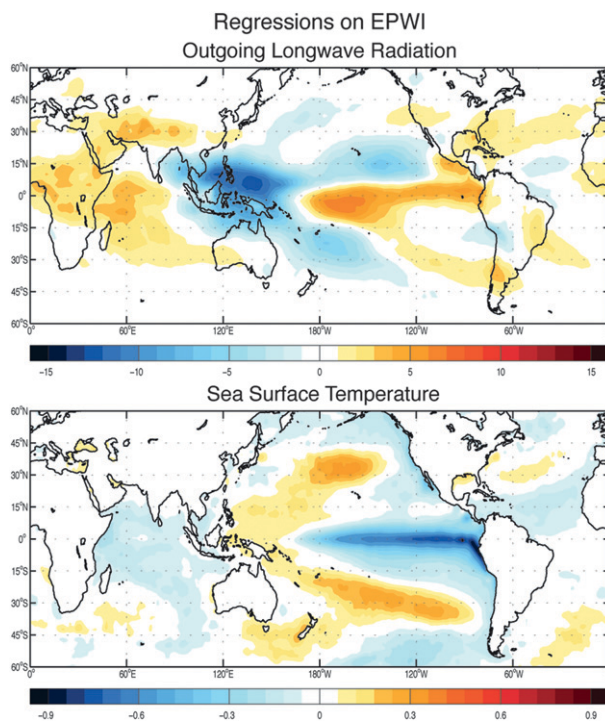

FIG. 7. Regressions on the EPWI time series: (top) daily mean outgoing longwave radiation anomalies and (bottom) monthly mean sea surface temperature anomalies. The contour interval is (top) 1 W m^{-2} and (bottom) 0.06°C. Units are per standard deviation in the EPWI time series. The bottom panel and all subsequent panels that use SST data are based on the period 1982–2009.

The bottom rows of Figs. 8 and 9 show the same fields as the top two rows, but in this case the basis for the regressions is inverted values of the ENSO index time series (Fig. 8, bottom row) and an index of the MJO (Fig. 9, bottom row). The ENSO index time series is inverted (i.e., multiplied by −1) so that the regression coefficients correspond to cold sea surface temperature anomalies in the eastern tropical Pacific Ocean. The index of the MJO is motivated by Fig. 10.

Figure 10 shows scatterplots of daily values of the EPWI time series plotted as a function of the orthogonal "RMM" MJO indices [the details of the indices are given in Wheeler and Hendon (2004)]. The top panel indicates days when the EPWI time series is greater than +1 standard deviation; the bottom panel indicates days when the EPWI time series is less than −1 standard deviation. Figure 10 illustrates that 1) enhanced amplitude in the equatorial planetary waves occurs with greatest frequency during MJO phases 5 and 6 (i.e., when the MJO is associated with peak and decaying convection just to the west of the International Date Line) and 2) suppressed amplitude in the equatorial planetary waves occurs with greatest frequency during MJO phases 1 and 2 (i.e., when convection is suppressed over the Maritime Continent and the western tropical Pacific Ocean). Thus, the strongest relationship between the MJO and the EPWI time series occurs along the diagonal axis through MJO phases 1, 2, 5, and 6. [Note that the MJO also has its greatest

influence on atmospheric angular momentum during similar phases; see previous work by Madden (1987) and Weickmann et al. (1997).] The regressions in the bottom row of Fig. 9 are based on the standardized sum of the paired RMM indices (i.e., RMM1 + RMM2) and hence correspond to regressions along the diagonal in Fig. 10.

Comparing the three rows in Figs. 8 and 9, it is clear that variability in the amplitude of the equatorial planetary waves not only emerges on intraseasonal and interannual time scales (middle rows) but also projects strongly onto ENSO (Fig. 8, bottom row) and the MJO during its phases 1, 2, 5, and 6 (Fig. 9, bottom row). In fact, roughly 60% of the variance in the EPWI time series can be explained by the combined influences of ENSO and the MJO. Patterns similar to those shown in Figs. 8 and 9 have been found in association with ENSO (e.g., Yulaeva and Wallace 1994; Seager et al. 2003; L'Heureux and Thompson 2006; Lu et al. 2008) and phases 5–6 of the MJO [cf. Figs. 8 and 9 of Wheeler and Hendon (2004); see also Fig. 4 of Hendon and Salby (1994)]. And the linkage between the equatorial planetary waves and ENSO was similarly confirmed in Dima and Wallace (2007). The primary differences between the structures in Figs. 8 and 9 are found in the subtropics, where the zonal-mean zonal wind
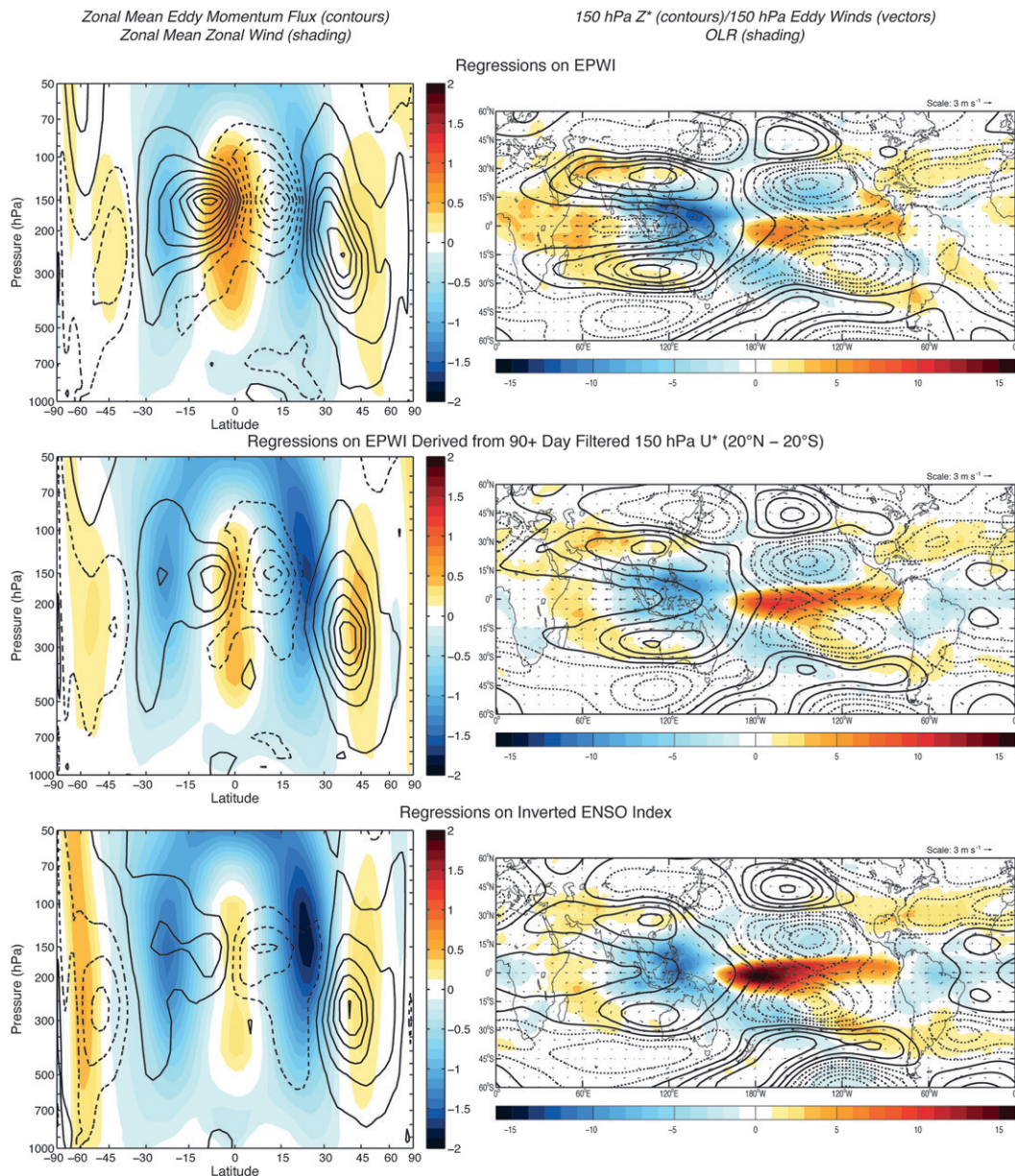
FIG. 8. Regressions on (top) the EPWI time series, (middle) the EPWI time series derived from the 90-day low-pass filtered daily-mean 150-hPa $U*$ anomalies for the region 20°N–20°S, and (bottom) the inverted (i.e., multiplied by −1) ENSO index time series. The black contours represent (left) zonal-mean eddy momentum flux anomalies and (right) 150-hPa $Z*$ anomalies. Positive contours are solid; negative contours are dashed. The contours are plotted at the same intervals as in Figs. 4 and 5. The colored shading represents (left) zonal-mean zonal wind anomalies and (right) OLR anomalies. The shading interval is (left) 0.125 m s^{-1} and (right) 1 W m^{-2}. The vectors in the right column represent 150-hPa eddy wind anomalies. Units are per standard deviation in each time series. The regressions on the ENSO index are performed using monthly mean anomalies.

anomalies are noticeably larger on interannual time scales (Fig. 8). The differences appear to be largely attributable to the greater extratropical eddy momentum fluxes observed in association with ENSO (Fig. 8, bottom left).

The high degree of resemblance between the structures associated with ENSO and the EPWI time series

reveals that variations in ENSO project strongly onto the amplitude of the equatorial planetary waves. The similar high degree of resemblance between the structures associated with the MJO and the EPWI time series suggests that the MJO can be viewed as consisting of two components: 1) a stationary component that is
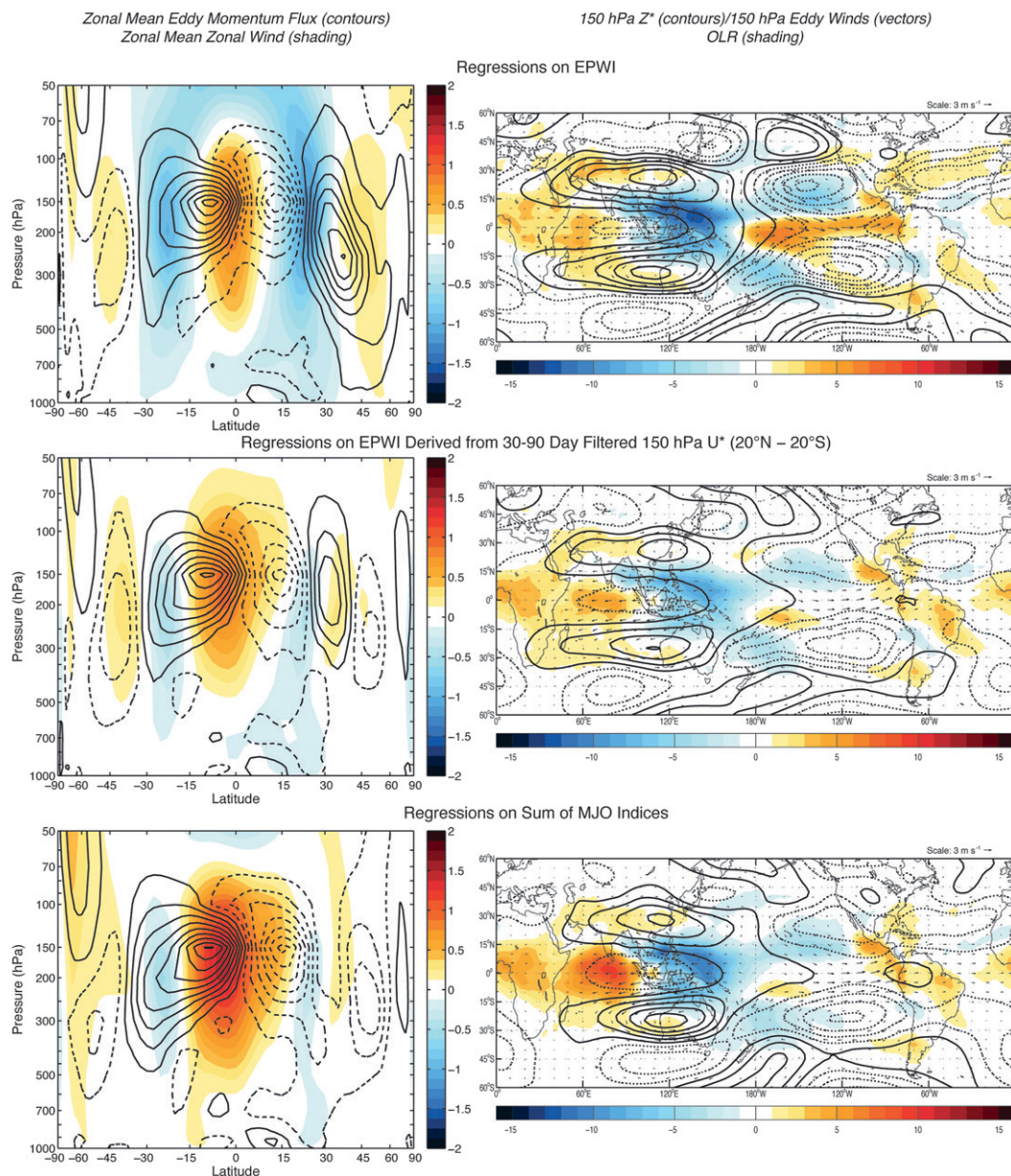
Zonal Mean Eddy Momentum Flux (contours)
Zonal Mean Zonal Wind (shading)

150 hPa Z* (contours)/150 hPa Eddy Winds (vectors)
OLR (shading)

Regressions on EPWI

Regressions on EPWI Derived from 30-90 Day Filtered 150 hPa U* (20°N – 20°S)

Regressions on Sum of MJO Indices

FIG. 9. As in Fig. 8, but for regressions on (middle) the EPWI time series derived from the 30–90-day bandpass filtered daily mean 150-hPa $U*$ anomalies for the region 20°N–20°S and (bottom) the sum of the paired MJO index time series. Units are per standard deviation in each time series.

linearly congruent with variability in the amplitude of the equatorial planetary waves and 2) a propagating component that is linearly unrelated to variability in the amplitude of the equatorial planetary waves. The decomposition of the MJO into these two components is shown in Fig. 11.

The left column of Fig. 11 shows the regressions of OLR, 150-hPa $Z*$, and 150-hPa eddy wind anomalies onto linear combinations of the Wheeler and Hendon (2004) RMM indices. The top panel corresponds to the

phase of the MJO that is characterized by anomalous convection to the south of India, and subsequent panels indicate the eastward progression of the anomalous convection across the Maritime Continent (e.g., see also Fig. 10). As documented extensively in the literature, the convective anomalies associated with the MJO are accompanied by upper tropospheric geopotential height anomalies that resemble the equatorial wave response to a localized tropical heating anomaly (e.g., Hendon and Salby 1994).
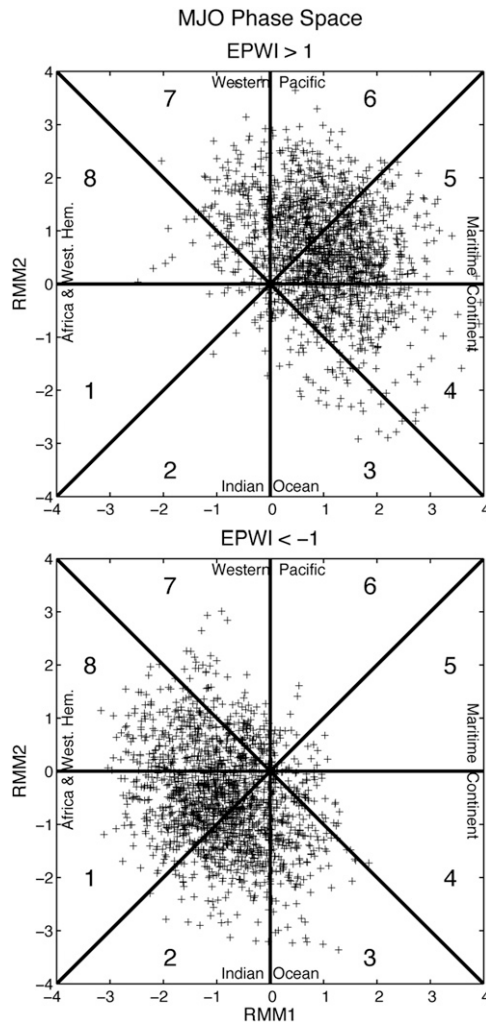
FIG. 10. Scatterplot of the phase space spanned by the paired MJO index time series (RMM1 and RMM2) for the days on which the EPWI time series is (top) greater than +1 standard deviation and (bottom) less than −1 standard deviation. The labels indicate the numerical phases of the MJO as defined in Wheeler and Hendon (2004) and the approximate location of the enhanced convection in each of those phases.

The middle column of Fig. 11 shows the contribution of the equatorial planetary waves to the structure of the MJO as a function of MJO phase; the right column shows the component of the MJO that is linearly uncorrelated with variability in the equatorial planetary waves (as defined by the EPWI time series). For each row in Fig. 11, the results are derived as follows: 1) the MJO index is regressed onto the EPWI time series and the resulting regression coefficient is multiplied by the EPWI time series to yield an EPWI congruent time series; 2) the EPWI congruent time series is subtracted from the total EPWI time series to yield a residual time series; and 3) daily OLR, 150-hPa Z^*, and 150-hPa eddy

winds are regressed onto the standardized congruent and residual time series. The resulting regression patterns are then scaled (i.e., multiplied by the correlation coefficients of the congruent and residual time series with the MJO index) such that the patterns in the right two columns of Fig. 11 sum to the pattern in the left column.

As noted earlier, the climatological-mean pattern of equatorial planetary waves does not project strongly onto the structure of the MJO when the anomalous convection is located over the eastern Indian Ocean (Fig. 10; second row of Fig. 11). But the projection is notable otherwise, particularly in the upper tropospheric Z^* field (top row and bottom two rows of Fig. 11). For example, when the anomalous convection is centered over the Maritime Continent (bottom two rows of Fig. 11), the equatorial planetary waves account for a substantial fraction of the structure of the MJO in the OLR, 150-hPa Z^*, and 150-hPa eddy wind fields (e.g., compare the left and middle columns in Fig. 11).

6. Linkages between the equatorial planetary waves and variability in stratospheric water vapor and the width of the tropics

In this section, we consider to what extent equatorial planetary waves contribute to two important aspects of tropical climate variability: stratosphere–troposphere exchange and the width of the tropical belt.

Previous studies have proposed a link between upwelling at the tropical tropopause and equatorial planetary waves (e.g., Boehm and Lee 2003; Norton 2006; Randel et al. 2008). Previous studies have also argued that recent changes in western tropical Pacific sea surface temperatures have led to decreases in tropical tropopause temperatures and stratospheric water vapor concentrations, presumably via changes in atmospheric convection (e.g., Rosenlof and Reid 2008; Solomon et al. 2010). However, using the EPWI time series, we do not find a definitive link between variability in equatorial planetary waves and stratospheric water vapor concentrations. Figure 12 shows the regressions of daily-mean *Aura* MLS water vapor anomalies (averaged over 20°N–20°S) on the standardized EPWI time series for the period 2005–09. Periods of enhanced amplitude in the equatorial planetary waves are associated with reduced water vapor mixing ratios in the tropical upper troposphere that are reminiscent of the water vapor anomalies associated with the MJO (e.g., Mote et al. 1998, 2000). But the region of significant water vapor anomalies does not extend above the tropopause level (Fig. 12). Hence, based on our analyses, equatorial planetary waves do not appear to play a central role in driving variability in tropical stratospheric water vapor.

Regressions on MJO Indices
150 hPa Z* (contours)/150 hPa Eddy Winds (vectors)
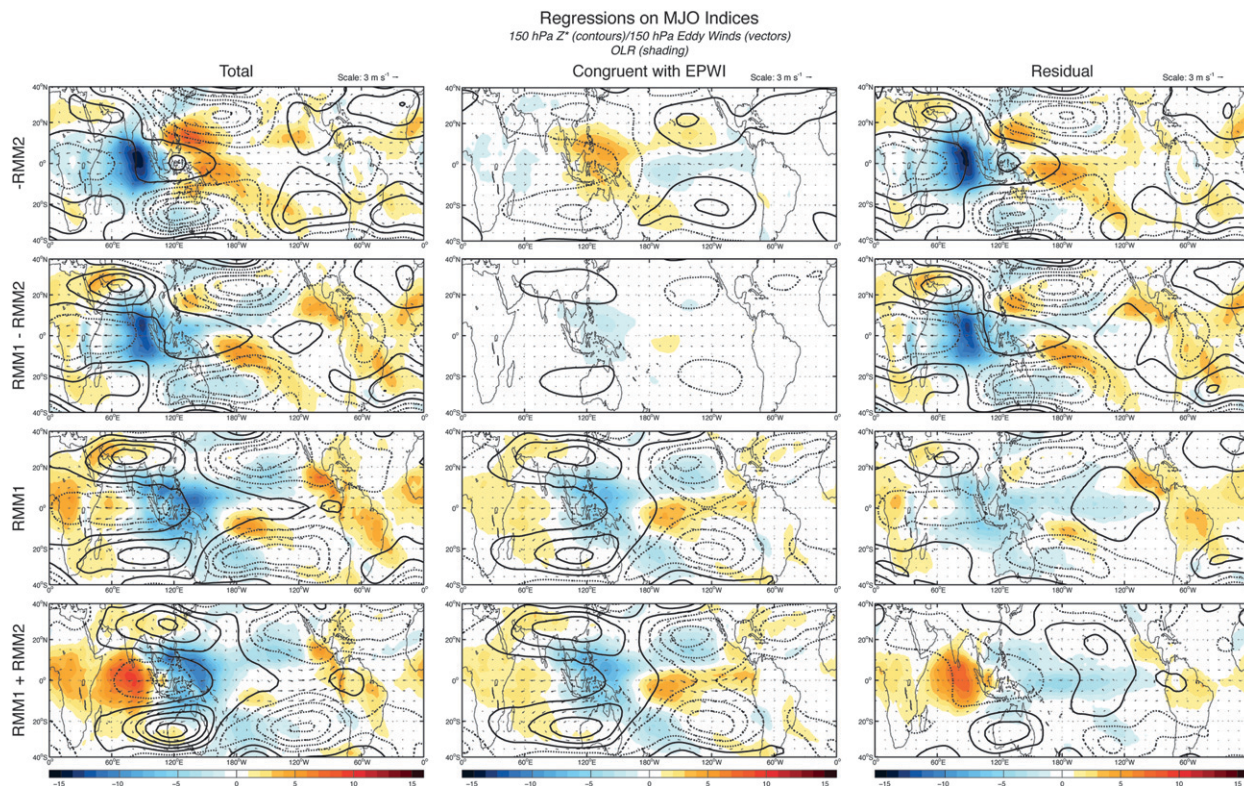OLR (shading)

FIG. 11. As in the right column of Fig. 8, but for regressions on linear combinations of the paired MJO indices (RMM1 and RMM2). The regressions are on (row 1) −RMM2, (row 2) RMM1 − RMM2, (row 3) RMM1, and (row 4) RMM1 + RMM2. (left) Total regressions, (middle) the component of the total regressions that is linearly congruent with the EPWI time series, and (right) the component of the total regressions that is linearly unrelated to the EPWI time series. Units are per standard deviation in the MJO indices.

Does variability in the equatorial planetary waves contribute to fluctuations in the width of the tropical belt (e.g., Fu et al. 2006; Seidel et al. 2008; Johanson and Fu 2009)? Figure 13 shows the regression onto the EPWI time series of two measures of the width of the tropics: the transition between zonal-mean easterlies and westerlies at the surface (top) and the 250 W m^{-2} OLR threshold used to denote the subtropical dry zones (bottom; e.g., Hu and Fu 2007). At first glance, variability in the equatorial planetary waves appears to have only a weak signature in both measures of the width of the tropics (Fig. 13). But on closer inspection, a +1 standard deviation change in the EPWI time series is associated with a widening of the tropical belt by approximately 0.7° latitude based on the surface wind measure (Fig. 13, top) and approximately 0.4° latitude based on the OLR measure (Fig. 13, bottom). The sign of the results is consistent with the relationships between ENSO and the width of the tropical belt (e.g., Seager et al. 2003; Lu et al. 2008) and between the MJO and the width of the Hadley circulation within select longitude bands (e.g., Hendon and Liebmann 1990a,b).

Figure 13 reveals that equatorial planetary waves are linked to changes in the width of the tropics on intraseasonal and interannual time scales. However, the EPWI time series does not exhibit statistically significant trends over the past few decades (not shown), and thus the contribution of equatorial planetary waves to decadal variability in the width of the tropics appears to be negligible, at least based on the decadal variability inherent in the EPWI time series derived from the NCEP–NCAR reanalysis. It is possible that equatorial planetary waves play a more prominent role in trends in the width of the tropics if reanalysis data underestimate the amplitude of the decadal variability in the EPWI time series.

7. Summary

Previous studies have established that equatorial planetary waves dominate the zonally asymmetric component of the climatological-mean tropical tropospheric circulation. The waves are forced by the latent heat release associated with deep convection and are dominated by an equatorially trapped Rossby wave response to the west of the convection over the western tropical Pacific Ocean and a Kelvin wave response to the east of the convection
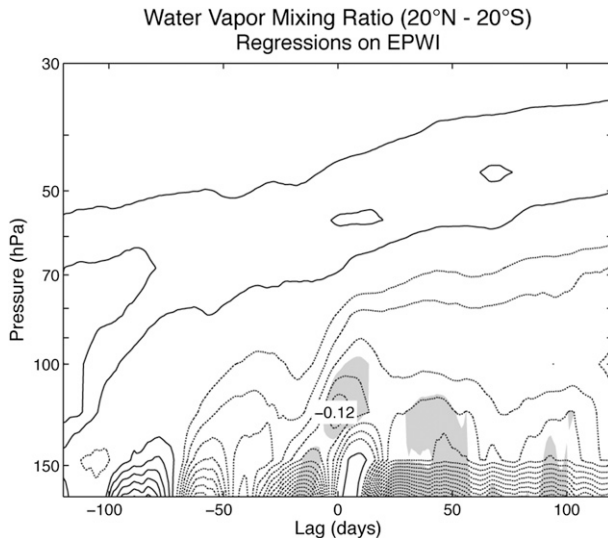
FIG. 12. Daily mean water vapor mixing ratio anomalies (averaged over 20°N–20°S) regressed on the EPWI time series. The EPWI leads (lags) the water vapor anomalies at positive (negative) lags. Positive contours are solid, negative contours are dashed, and the zero contour has been omitted. The contour interval is 0.02 ppmv. Units are per standard deviation in the EPWI time series. The shading indicates regions that are 95% significant. This figure is based on data covering the period 2005–09.

(e.g., Gill 1980; Highwood and Hoskins 1998; Dima et al. 2005; Dima and Wallace 2007). The equatorial planetary waves play an important role in the zonal-mean momentum balance of the tropics (Lee 1999; Dima et al. 2005; Kraucunas and Hartmann 2005) and are potentially important for tropical stratosphere–troposphere exchange (e.g., Boehm and Lee 2003; Norton 2006; Randel et al. 2008).

In this paper, we have established that equatorial planetary waves play an equally prominent role in atmospheric variability. Temporal variability in the amplitude of the climatological-mean pattern of equatorial planetary waves was identified by projecting daily anomalies of the eddy zonal wind field in the tropics onto its seasonally varying climatological-mean values. The resulting projection time series (referred to herein as the equatorial planetary wave index, or EPWI, time series) captures coherent large-scale variability in the amplitude of the equatorial planetary waves throughout the tropics. The structure of the equatorial planetary waves in atmospheric variability also emerges from one-point correlation maps and from EOF analysis of a range of key tropical dynamical fields, suggesting that the waves reflect a unique pattern of tropical climate variability in their own right.

Variations in the amplitude of the equatorial planetary waves (as characterized by the EPWI time series) are
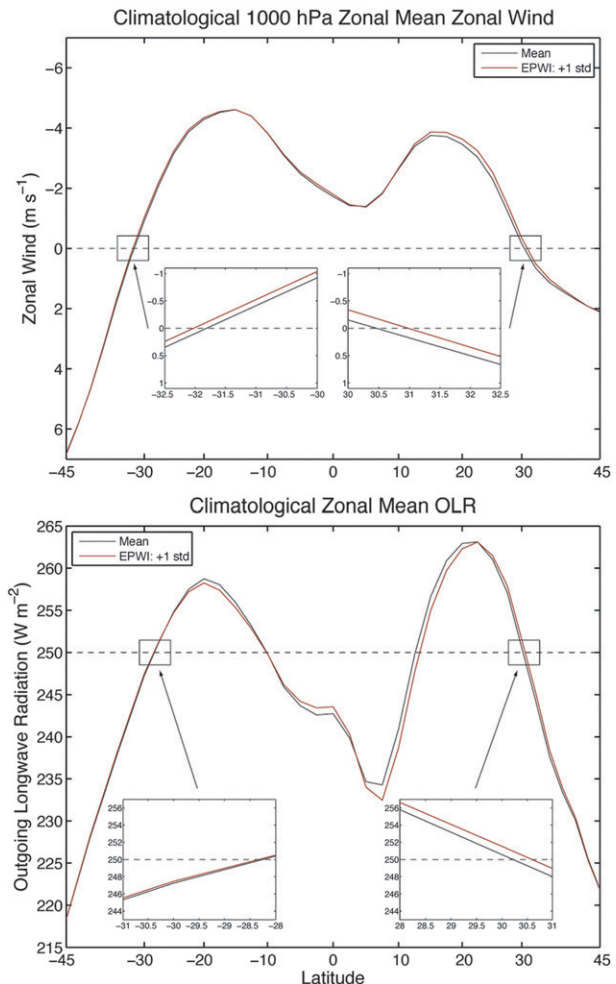

FIG. 13. Climatological zonal-mean (top) 1000-hPa zonal wind and (bottom) OLR. The climatological-mean values (solid black line) are accompanied by the regressions of daily mean, zonal-mean (top) 1000-hPa zonal wind anomalies and (bottom) OLR anomalies on the EPWI time series. The regression coefficients have been added to the climatological-mean values at each latitude (red line). The dashed line indicates the (top) 0 m s^{-1} and (bottom) 250 W m^{-2} thresholds. Note that the ordinate is reversed in the top panel to emphasize easterly winds.

associated with a range of tropical circulation anomalies that are reminiscent of the simulated response to zonally asymmetric tropical heating (e.g., Gill 1980; Highwood and Hoskins 1998; Kraucunas and Hartmann 2005; Norton 2006). The positive polarity of the EPWI time series (i.e., enhanced amplitudes of the equatorial planetary waves) is associated with 1) equatorially symmetric eddy momentum flux anomalies that converge about the equator in the upper troposphere, 2) westerly upper tropospheric wind anomalies centered about the equator, 3) negative temperature anomalies in the tropical and subtropical lower stratosphere, 4) deep easterly wind anomalies centered near 25° latitude in both hemispheres, and 5) positive

temperature anomalies throughout the depth of the Northern and Southern Hemisphere subtropical troposphere (Figs. 4 and 5). The zonal-mean temperature and wind anomalies associated with variations in the equatorial planetary waves are consistent with the zonal-mean balanced response to the equatorially symmetric eddy momentum flux anomalies in the tropical upper troposphere (Figs. 4 and 6).

The positive polarity of the EPWI time series is also marked by enhanced convection over the Maritime Continent and western tropical Pacific Ocean, suppressed convection over the Indian Ocean and eastern tropical Pacific Ocean, and sea surface temperature anomalies that are reminiscent of the cold phase of the ENSO cycle (Fig. 7). Thus, the equatorial planetary waves project strongly onto not only ENSO, but also onto the MJO during periods when the anomalous convection is centered near the Maritime Continent (Figs. 8 and 9). As a result, we have suggested that the MJO can be viewed as the linear superposition of two distinct components: 1) a stationary component that is linearly congruent with variability in the amplitude of the equatorial planetary waves and 2) a propagating component that is linearly unrelated to variability in the amplitude of the equatorial planetary waves. Past studies have shown that the MJO cannot be interpreted solely as a Kelvin wave (e.g., Hsu 1996; Zhang 2005). They have also shown that the MJO cannot be thought of as a standing oscillation in convection that excites a propagating circulation anomaly (Zhang and Hendon 1997). But the results shown here suggest that the equatorial planetary waves excited by the MJO may act to alias the propagating signature of the MJO. The implications of the results for theories of the MJO remain to be determined.

Variability in the equatorial planetary waves is also important for interpreting other aspects of tropical climate variability. The weak signature of the equatorial planetary waves in tropical tropopause temperatures (Fig. 4, bottom left) suggests that they may play a role in driving variability in troposphere–stratosphere exchange (see also Norton 2006). However, we have shown that the equatorial planetary waves are not strongly linked to variations in stratospheric water vapor. The equatorial planetary waves contribute to intraseasonal and interannual variability in the width of the tropics (Fig. 13), but they have not contributed to trends in the width of the tropics (at least based on trends in the reanalysis data). More detailed analyses will be necessary to determine the relevance of equatorial planetary waves for these and other forms of tropical decadal climate variability.

Overall, the results of this paper reveal that the pulsation of the quasi-stationary equatorial planetary waves

provides a framework for interpreting the tropical response to a range of climate phenomena. Future studies might consider the role of the equatorial planetary waves when interpreting low-frequency variability in the tropical climate system.

REFERENCES

Boehm, M. T., and S. Lee, 2003: The implications of tropical Rossby waves for tropical tropopause cirrus formation and for the equatorial upwelling of the Brewer–Dobson circulation. *J. Atmos. Sci.,* **60,** 247–261.

Bretherton, C. S., M. Widmann, V. P. Dymnikov, J. M. Wallace, and I. Bladé, 1999: The effective number of spatial degrees of freedom of a time-varying field. *J. Climate,* **12,** 1990–2009.

Dima, I. M., and J. M. Wallace, 2007: Structure of the annual-mean equatorial planetary waves in the ERA-40 reanalyses. *J. Atmos. Sci.,* **64,** 2862–2880.

——, ——, and I. Kraucunas, 2005: Tropical zonal momentum balance in the NCEP reanalyses. *J. Atmos. Sci.,* **62,** 2499–2513.

Dunkerton, T. J., 1995: Evidence of meridional motion in the summer lower stratosphere adjacent to monsoon regions. *J. Geophys. Res.,* **100,** 16 675–16 688.

Edmon, H. J., B. J. Hoskins, and M. E. McIntyre, 1980: Eliassen–Palm cross sections for troposphere. *J. Atmos. Sci.,* **37,** 2600–2616.

Fu, Q., C. M. Johanson, J. M. Wallace, and T. Reichler, 2006: Enhanced mid-latitude tropospheric warming in satellite measurements. *Science,* **312,** 1179.

Gill, A. E., 1980: Some simple solutions for heat-induced tropical circulation. *Quart. J. Roy. Meteor. Soc.,* **106,** 447–462.

Hendon, H. H., and B. Liebmann, 1990a: The intraseasonal (30–50 day) oscillation of the Australian summer monsoon. *J. Atmos. Sci.,* **47,** 2909–2923.

——, and ——, 1990b: A composite study of onset of the Australian summer monsoon. *J. Atmos. Sci.,* **47,** 2227–2240.

——, and M. L. Salby, 1994: The life cycle of the Madden–Julian oscillation. *J. Atmos. Sci.,* **51,** 2225–2237.

Highwood, E. J., and B. J. Hoskins, 1998: The tropical tropopause. *Quart. J. Roy. Meteor. Soc.,* **124,** 1579–1604.

Hoerling, M. P., A. Kumar, and T. Xu, 2001: Robustness of the nonlinear climate response to ENSO's extreme phases. *J. Climate,* **14,** 1277–1293.

Holton, J. R., P. H. Haynes, M. E. McIntyre, A. R. Douglass, R. B. Rood, and L. Pfister, 1995: Stratosphere–troposphere exchange. *Rev. Geophys.,* **33,** 403–439.

Hsu, H.-H., 1996: Global view of the intraseasonal oscillation during northern winter. *J. Climate,* **9,** 2386–2406.

Hu, Y., and Q. Fu, 2007: Observed poleward expansion of the Hadley circulation since 1979. *Atmos. Chem. Phys.,* **7,** 5229–5236.

Johanson, C. M., and Q. Fu, 2009: Hadley cell widening: Model simulations versus observations. *J. Climate,* **22,** 2713–2725.

Kalnay, E., and Coauthors, 1996: The NCEP/NCAR 40-Year Reanalysis Project. *Bull. Amer. Meteor. Soc.,* **77,** 437–471.

Kerr-Munslow, A. M., and W. A. Norton, 2006: Tropical wave driving of the annual cycle in tropical tropopause temperatures. Part I: ECMWF analyses. *J. Atmos. Sci.,* **63,** 1410–1419.

Kistler, R., and Coauthors, 2001: The NCEP–NCAR 50-Year Reanalysis: Monthly means CD-ROM and documentation. *Bull. Amer. Meteor. Soc.,* **82,** 247–267.

Kraucunas, I., and D. L. Hartmann, 2005: Equatorial superrotation and the factors controlling the zonal-mean zonal winds in the tropical upper troposphere. *J. Atmos. Sci.,* **62,** 371–389.

Lambert, A., and Coauthors, 2007: Validation of the Aura Microwave Limb Sounder middle atmosphere water vapor and nitrous oxide measurements. *J. Geophys. Res.,* **112,** D24S36, doi:10.1029/2007JD008724.

Lee, S., 1999: Why are the climatological zonal winds easterly in the equatorial upper troposphere? *J. Atmos. Sci.,* **56,** 1353–1363.

L'Heureux, M. L., and D. W. J. Thompson, 2006: Observed relationships between the El Niño–Southern Oscillation and the extratropical zonal-mean circulation. *J. Climate,* **19,** 276–287.

Liebmann, B., and C. A. Smith, 1996: Description of a complete (interpolated) outgoing longwave radiation dataset. *Bull. Amer. Meteor. Soc.,* **77,** 1275–1277.

Lu, J., G. Chen, and D. M. W. Frierson, 2008: Response of the zonal mean atmospheric circulation to El Niño versus global warming. *J. Climate,* **21,** 5835–5851.

Madden, R. A., 1987: Relationships between changes in the length of day and the 40- to 50-day oscillation in the tropics. *J. Geophys. Res.,* **92,** 8391–8399.

Mote, P. W., T. J. Dunkerton, and H. C. Pumphrey, 1998: Subseasonal variations in lower stratospheric water vapor. *Geophys. Res. Lett.,* **25,** 2445–2448.

——, H. L. Clark, T. J. Dunkerton, R. S. Harwood, and H. C. Pumphrey, 2000: Intraseasonal variations of water vapor in the tropical upper troposphere and tropopause region. *J. Geophys. Res.,* **105,** 17 457–17 470.

Norton, W. A., 2006: Tropical wave driving of the annual cycle in tropical tropopause temperatures. Part II: Model results. *J. Atmos. Sci.,* **63,** 1420–1431.

Randel, W. J., R. Garcia, and F. Wu, 2008: Dynamical balances and tropical stratospheric upwelling. *J. Atmos. Sci.,* **65,** 3584–3595.

Rasmusson, E. M., and T. H. Carpenter, 1982: Variations in tropical sea surface temperature and surface wind fields associated with the Southern Oscillation/El Niño. *Mon. Wea. Rev.,* **110,** 354–384.

Read, W. G., and Coauthors, 2007: Aura Microwave Limb Sounder upper tropospheric and lower stratospheric H_2O and relative humidity with respect to ice validation. *J. Geophys. Res.,* **112,** D24S35, doi:10.1029/2007JD008752.

Reynolds, R. W., N. A. Rayner, T. M. Smith, D. C. Stokes, and W. Wang, 2002: An improved in situ and satellite SST analysis for climate. *J. Climate,* **15,** 1609–1625.

Rosenlof, K. H., and G. C. Reid, 2008: Trends in the temperature and water vapor content of the tropical lower stratosphere: Sea surface connection. *J. Geophys. Res.,* **113,** D06107, doi:10.1029/2007JD009109.

Ryu, J.-H., and S. Lee, 2010: Effect of tropical waves on the tropical tropopause transition layer upwelling. *J. Atmos. Sci.,* **67,** 3130–3148.

Seager, R., N. Harnik, Y. Kushnir, W. Robinson, and J. Miller, 2003: Mechanisms of hemispherically symmetric climate variability. *J. Climate,* **16,** 2960–2978.

Seidel, D. J., Q. Fu, W. J. Randel, and T. J. Reichler, 2008: Widening of the tropical belt in a changing climate. *Nat. Geosci.,* **1,** 21–24.

Simmons, A. J., and B. J. Hoskins, 1978: The life cycles of some nonlinear baroclinic waves. *J. Atmos. Sci.,* **35,** 414–432.

Solomon, S., K. H. Rosenlof, R. W. Portmann, J. S. Daniel, S. M. Davis, T. J. Sanford, and G.-K. Plattner, 2010: Contributions of stratospheric water vapor to decadal changes in the rate of global warming. *Science,* **327,** 1219–1223.

Ueyama, R., and J. M. Wallace, 2010: To what extent does high-latitude wave forcing drive tropical upwelling in the Brewer–Dobson circulation? *J. Atmos. Sci.,* **67,** 1232–1246.

Weickmann, K. M., G. N. Kiladis, and P. D. Sardeshmukh, 1997: The dynamics of intraseasonal atmospheric angular momentum oscillations. *J. Atmos. Sci.,* **54,** 1445–1461.

Wheeler, M. C., and H. H. Hendon, 2004: An all-season real-time multivariate MJO index: Development of an index for monitoring and prediction. *Mon. Wea. Rev.,* **132,** 1917–1932.

Yulaeva, E., and J. M. Wallace, 1994: The signature of ENSO in global temperatures and precipitation fields derived from the Microwave Sounding Unit. *J. Climate,* **7,** 1719–1736.

——, J. R. Holton, and J. M. Wallace, 1994: On the cause of the annual cycle in tropical lower-stratospheric temperatures. *J. Atmos. Sci.,* **51,** 169–174.

Zhang, C., 2005: Madden-Julian oscillation. *Rev. Geophys.,* **43,** RG2003, doi:10.1029/2004RG000158.

——, and H. H. Hendon, 1997: Propagating and standing components of the intraseasonal oscillation in tropical convection. *J. Atmos. Sci.,* **54,** 741–752.